Localization and Molecular Interactions of Mitoxantrone within Living K562 Cells as Probed by Confocal Spectral Imaging Analysis

Alexei Feofanov,* Serguei Sharonov,# Irina Kudelina,* Fabrice Fleury,# and Igor Nabiev#
*Shemyakin and Ovchinnikov Institute of Bioorganic Chemistry, Russian Academy of Sciences, 117871 Moscow, Russia, and #Laboratoire de Spectroscopie Biomoléculaire, UFR de Pharmacie, Université de Reims Champagne-Ardenne, 51096 Reims Cedex, France

ABSTRACT Studying mechanisms of drug antitumor action is complicated by the lack of noninvasive methods enabling direct monitoring of the state and interactions of the drugs within intact viable cells. Here we present a confocal spectral imaging (CSI) technique as a method of overcoming this problem. We applied this method to the examination of localization and interactions of mitoxantrone (1, 4-dihydroxy-5, 8-bis-{{[2-(2-hydroxyethyl)-amino]ethyl}amino}-9,10-anthracenedione dihydrochloride), a potent antitumor drug, in living K562 cells. A two-dimensional set of fluorescence spectra of mitoxantrone (MITOX) recorded with micron resolution within a drug-treated cell was analyzed to reveal formation of drug-target complexes and to create the maps of their intracellular distribution. The analysis was based on detailed in vitro modeling of drug-target (DNA, RNA, DNA topoisomerase II) interactions and environmental effects affecting drug fluorescence. MITOX exposed to aqueous intracellular environment, MITOX bound to hydrophobic cellular structures, complexes of MITOX with nucleic acids, as well as the naphtoquinoxaline metabolite of MITOX were simultaneously detected and mapped in K562 cells. These states and complexes are known to be immediately related to the antitumor action of the drug. The results obtained present a basis for the subsequent quantitative analysis of concentration and time-dependent accumulation of free and bound MITOX within different compartments of living cancer cells.

INTRODUCTION

Preclinical screening and investigation of new drugs for chemotherapy is directly related to the identification of critical biochemical targets and analysis of cellular factors responsible for cytotoxic action of the drugs. The combined application of conventional biochemical and cytological methods with noninvasive quantitative techniques such as flow cytometry and laser scanning confocal fluorescence microscopy (LSCFM) may be considered the most effective approach to determining the cytotoxic potential and pharmacological features of antitumor drugs.

Flow cytometry and LSCFM are widely used to examine the uptake and localization of fluorescent compounds or labeled fluorescence probes in intact, viable cells (Pawley, 1990; McLean Grogan and Collins, 1990). These techniques analyze an integral fluorescence signal selected by the broad-band filter. When spectral parameters of a fluorescence probe are known to be unchanged, or (the opposite) they change considerably and specifically because of intracellular interactions, the flow cytometry and LSCFM enable precise quantitative analysis. By the use of a set of different filters, the interactions and/or environmental characteristics of specific fluorescence probes with well-separated spectral characteristics may be simultaneously recognized in cells.

Received for publication 29 May 1997 and in final form 19 September 1997.

Address reprint requests to Prof. Igor Nabiev, Laboratoire de Spectroscopie Biomoléculaire, UFR de Pharmacie, Université de Reims Champagne-Ardenne, 51, rue Cognacq Jay, 51096 Reims, France. Tel.: 333-26053554; Fax: 333-26826001; E-mail: igor.nabiev@univ-reims.fr.

0006-3495/97/12/3317/11 $2.00

More generally, when interactions of fluorophores are manifested only by subtle spectral changes, their identification is more ambiguous. Yet particular intracellular interactions of such fluorophores like, for example, anticancer drugs, may be of great interest. Indeed, when the signals from drug-target complexes, a free drug, and the cell intrinsic fluorescence overlap, they cannot be separated and identified with the restricted set of broad-band filters.

Recently a new approach based on confocal spectral imaging (CSI) analysis has been developed (Sharonov et al., 1994a,b; Feofanov et al., 1995). Combining a laser confocal scanning microscope with a spectrograph and a charge coupled device (CCD) detection system, the CSI technique allows the 2D set of spectra to be recorded with submicron 3D spatial resolution from an intact living cell treated with a fluorescent drug. To create the spectral images describing subcellular localization and interactions of a drug, the decomposition procedure should be applied to the set of the recorded spectra. According to this procedure, each original spectrum is decomposed into a sum of the reference spectra with appropriate coefficients. The reference spectra originating from in vitro modeling are attributed to different states and specific interactions of the fluorophore. Such an approach also enables enhancement/quenching of fluorescence of the drug localized in different states to be taken into account. This advantage of the CSI technique is extremely important for correct analysis, but it is not a property of either flow cytometry or LSCFM if the analyzed signals overlap.

As compared to the "similarity mapping procedure" realized recently (Malik et al., 1996), the spectral decomposition technique is more general and convenient. The "sim-

ilarity mapping procedure" calculates the degree of difference between the shape of the experimental spectrum at the current point of the sample and the shape of a single reference spectrum and creates 2D maps of similarity. The real intensity of the experimental spectrum, which characterizes the concentration of a fluorophore, is omitted in this approach. Moreover, when the coefficient of similarity is not unity, the contribution of the reference spectrum is not clear. In a general case, an experimental spectrum is a superposition of several states and their relative contributions are quite important, but cannot be identified by using the "similarity mapping procedure." Nevertheless, this approach is well suited to assigning a measured signal to one of several possible reference signals (Liyanage et al., 1996).

In our preliminary report (Sharonov et al., 1994a), the CSI technique was demonstrated to be useful in the study of the antitumor agent mitoxantrone (1,4-dihydroxy-5,8-bis-{{[2-(2-hydroxyethyl)-amino]ethyl}amino}-9,10-anthracenedione dihydrochloride; NSC301739). Mitoxantrone (Novatrone), a synthetic anthraquinone drug (Fig. 1), shows considerable activity against a wide variety of animal tumor models (Fujimoto and Ogawa, 1982; Johnson et al., 1979), as well as in the clinical treatment of acute nonlymphocytic leukemia, advanced breast cancer, and non-Hodgkin's lymphomas (Arlin et al., 1990; Ehninger et al., 1990; Faulds et al., 1991). The exact mechanisms responsible for the antitumor action of mitoxantrone (MITOX) have yet not been elucidated. There may be a number of mechanisms involving the formation of MITOX-DNA complexes (Smith et al., 1990; Kapuscinski et al., 1986), complexes of MITOX with cytoskeleton proteins (Roberts et al., 1989; Ho et al., 1991), and/or accumulation of cytotoxic metabolites (Mewes et al., 1993). Here we apply the CSI technique to direct monitoring of localization and interactions of MITOX within living cells. We are starting from a detailed study of environmental factors and molecular interactions affecting the parameters of MITOX fluorescence. The considerable sensitivity of MITOX fluorescence to interactions and environmental factors revealed in this work demonstrates that in vitro modeling of drug-target interactions should be regarded as an important primary step toward the situ study of drug uptake, distribution, and interactions. It predetermines the correct use of the CSI technique, as well as flow cytometry and LSCFM for drug analysis in living cells.

Based on the results of in vitro modeling, several states and interactions of MITOX within K562 cells were identified by the CSI technique: MITOX in an aqueous environment, MITOX bound to hydrophobic cellular structures, and MITOX bound to nucleic acids. The naphtoquinoxaline metabolite of MITOX was also detected in drug-treated cells. The basis set of the reference spectra, which is well suited to describing the state and interactions of MITOX, was obtained, and it was proved to be adequate in determining the accumulation and localization of MITOX in K562 cells.

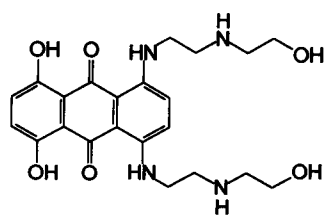

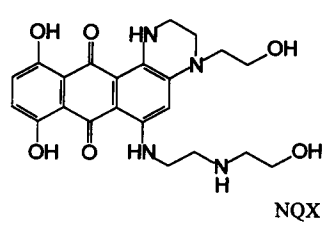

FIGURE 1 Structure of MITOX and its naphthoquinoxaline metabolite (NQX).

MATERIALS AND METHODS

Enzymes, nucleic acids, and reagents

Calf thymus DNA, calf liver RNA (type IV), horseradish peroxidase (crude), and Triton X-100 (t-octylphenoxypolyethoxyethanol) were purchased from Sigma (St. Louis, MO) and used as received. Calf thymus DNA topoisomerase II (0.18×10^6 units/mg) was a gift of Rhone-Poulenc Rorer, S.A. (France). One unit of topoisomerase II (topo II) was defined as described earlier (Nabiev et al., 1994). Mitoxantrone was a gift of Léderlé Laboratories (Rungis). A stock solution (0.1 mM) of MITOX was prepared in phosphate-buffered saline (PBS) for both cell treatments and in vitro experiments. Concentration of MITOX in the aqueous buffer solutions was measured by absorption at the isosbestic point at $\lambda_i = 682$ nm, using the extinction coefficient $\epsilon_{\lambda i} = 8.36 \times 10^3\ M^{-1}\ cm^{-1}$ (Kapuscinski et al., 1981). It should be mentioned that MITOX adsorbs thoroughly (2×10^{-10} mol/cm^2) at the walls of a plastic culture dish. Accordingly, appropriate correction was made for the drug concentration when working with a $\sim 10^{-6}$ M concentration of the drug.

All other chemicals were of analytical-reagent grade, and all solvents were of high-performance liquid chromatography grade.

Cells

K562 is a human erythroleukemic cell line, established from a patient with chronic myelogeneous leukemia in blast transformation. Cells were grown exponentially at $3–7 \times 10^5$ cells/ml in RPMI-1640 (Gibco, Grand Island, NY) containing 10% fetal calf serum (Seromed) and 2 mM L-glutamine (Sigma). After the incubation with MITOX (10 μM drug for 1 h or 2 μM drug for 1 h), the cells were rinsed two times with PBS, resuspended with fresh PBS, and placed under a microscope for measurement.

Preparation of complexes and reaction mixtures for in vitro modeling experiments

The concentration of DNA (RNA) in the solution was 113 μM (97 μM) in base pairs. Drug-DNA and drug-RNA complexes were prepared by mixing the components in PBS buffer at the initial MITOX/DNA and MITOX/RNA molar ratios of 1/100 bp and 1/80 bp, respectively. The titration procedure was performed by incrementally adding MITOX from the stock solution to reach the final drug/DNA and drug/RNA molar ratios of 1/10 bp and 1/14 bp, respectively. The concentration of DNA was determined by absorption at 260 nm ($\epsilon = 6600\ M^{-1}$ (bp) cm^{-1}).

The ternary cleavable complexes of MITOX with topo II and DNA were prepared in the 50-μl final reaction volume of PBS containing 4 μM MITOX, 50 units of topo II, and 240 μM DNA. The components were mixed at 4°C and incubated at 37°C for 20 min, and then a drop of reaction mixture was placed under the microscope.

Oxidation of MITOX by horseradish peroxidase was initiated by mixing a 2-ml solution of PBS containing 10 μM MITOX and 80 μM hydrogen peroxide with 2 μl of the enzyme (1 mg/ml). Reaction was self-terminated by reaching the equilibrium state after ~20 min. The further oxidation of MITOX did not occur during the next 3–4 h, as was detected by absorption. Formation of the naphthoquinoxaline (NQX) derivative of MITOX was confirmed by the appearance of the characteristic absorption spectrum of NQX with maxima at 584 and 628 nm (Reszka et al., 1986) instead of the spectrum of MITOX. Numerical decomposition (Gigli et al., 1988) of the fluorescence spectrum measured from the reaction mixture led us to the conclusion that the ~4/1 molar ratio was achieved between NQX and MITOX at the equilibrium state.

To probe the disturbance of MITOX spectral parameters in the presence of topo II, 50 units of the enzyme was added to the 50-μl final reaction volume of PBS containing 4 μM MITOX.

Detergent-containing solutions of MITOX (10 μM) were prepared at the critical micelle concentration of Triton X-100 (0.24 mM) in the PBS buffer. Solutions of MITOX (10 μM) were also prepared at 4 mM and 50 mM concentrations of Triton X-100.

Solutions of MITOX in methanol, ethanol, and propanol as well as a solution of NQX in dioxane were prepared at the drug concentration of 10 μM.

Spectral measurements

Fluorescence spectra were measured with a Hitachi MPF-3 fluorimeter (Japan). Circular dichroism (CD) spectra were recorded with a Jasco-500C dichrograph (Japan), and a Cary-209 spectrophotometer (Varian, Sunnyvale, CA) was used for absorption measurements. Microfluorescence analysis of solutions and CSI measurements of cells were performed with a modular Raman/fluorescence XY-500 spectrometer (DILOR, France) equipped with a microscope (Olympus BH2, Japan), confocal entrance chamber, and a system of galvanometer-controlled mirror scanners (Feofanov et al., 1995). Microfluorescence measurements were carried out with a 100× phase contrast objective (Olympus UVFL100PL). The spectral resolution was 0.15 nm. The spatial resolution was ~1 μm (lateral resolution) and ~3 μm (axial resolution). Spectral images were accumulated and treated as described previously (Feofanov et al., 1995; Sharonov et al., 1994a,b).

Briefly, the focused laser beam scanned a specimen along a line. The fluorescence signal emitted by the specimen was decomposed after confocal filtration by the spectrometer into a spectrum and detected by CCD camera. The spectra from different points of the specimen scanning line were projected onto different rows of CCD pixels. The whole 2D set of spectra was recorded by the line-by-line scanning method. To create the 2D spectral images presented in this paper, a spectrum decomposition procedure or a procedure based on the integration of the signal over the selected spectral region was applied.

The spectrum decomposition procedure was based on the deconvolution of each experimental spectrum into a sum of the reference spectra with appropriate coefficients. The least-squares linear regression algorithm was employed to calculate decomposition coefficients. 2D maps of the decomposition coefficients (hereafter referred to as spectral images) describe the relative distribution along the specimen of each component; the spectrum of each component was introduced as a reference. The reference spectra were taken from in vitro modeling measurements. The validity of the performed procedure was proved by calculating a map of errors for each decomposition.

The 50 × 50 or 40 × 40 pixel spectral images were recorded with the 514.5-nm excitation wavelength of an Ar^+ laser (model 2020-03; Spectra Physics) at 0.1 mW. The recording time of a spectral image did not exceed 4 min. Neither bleaching of intracellular MITOX nor disturbance of cellular structure was observed under the experimental conditions used. By repeating image measurements, we could ascertain that probing of the drug-target interactions with a laser beam affected neither the initial pattern of the drug distribution and interactions, nor the intact cellular structure. It was found that the influence of laser radiation on a cell appeared only after several (usually 5–7) repetitions of image recording (20–28 min of irradiation).

RESULTS

In vitro studies of MITOX interactions by fluorescence, absorption, and CD techniques

Dimerization of MITOX in water solution

Increasing concentration leads to dimerization of MITOX molecules ($K_d = 3 \times 10^4$ M^{-1}) in water solution (Kapuscinski and Darzynkiewicz, 1985). The dimers are detected by measuring the ratio of intensities at the long- and short-wavelength absorption maxima (R_A) of MITOX (Table 1). The R_A ratio equal to 1.33–1.36 for monomeric MITOX is reduced significantly because of dimer formation (Kapuscinski and Darzynkiewicz, 1985). The dimerization drastically changes the concentration of monomeric MITOX from ~95% at a total drug concentration (C_{tot}) of 1 μM to ~34% at C_{tot} = 0.1 mM. The dependence of the fluorescence intensity on C_{tot} measured by microspectrofluorometry and corrected for the effect of the inner filter reveals a saturation (Fig. 2 *a*). On the other hand, the fluorescence intensity is directly proportional to the concentration of monomeric MITOX in solution (Fig. 2 *a*). The positions of the maximum (λ_{max} = 685 nm) and the shape of the emission spectrum corrected for reabsorption of the emitted light are independent of dimer content in solution. Moreover, the shape of the excitation spectrum is very similar to that of the absorption spectrum of monomeric MITOX (Fig. 2 *b*). These observations suggest that the dimers of MITOX do not fluoresce, so that only the monomeric form of the drug contributes to the fluorescence spectrum.

The drug aggregation depends on the pH of the solution increasing sharply, producing a basic environment (Table 1). It is detected by a remarkable decrease in both fluorescence intensity and the R_A coefficient, which occurs on going from a neutral (pH 7.4) to a basic (pH 10) environment. The aggregation was found to be reversible, and should be related to deprotonation of NH_3^+ groups of the aminoalkylamino side chains at basic pH. A pH decrease from 7.4 to 4.0 is followed by only a slight fluorescence increase (Table 1). In a similar manner, a small increase in the drug fluorescence may occur in acidic compartments of the cell as well as in the microenvironment, where the local pH is reduced. The position of the maximum and the shape of the emission spectrum are not affected by pH.

Effect of solvent polarity and interactions with hydrophobic micelles

The influence of environment polarity on the spectral properties of MITOX was studied by comparing the spectra of

TABLE 1 Spectral parameters of absorption and fluorescence spectra of mitoxantrone and its naphtoquinoxaline metabolite in different environmental conditions, complexes, and mixtures

	Absorption			Fluorescence#		
Solvent, conditions*	λ_{max1} (nm)	λ_{max2} (nm)	R_A§	λ_{max} (nm)	FWHM¶ (nm)	I_{rel}‖
MITOX, 100% monomers,** PBS (pH 7.4)	610	661	1.34	685	58	1.0
MITOX, PBS (pH 10)	614	665	0.56	685	58	0.08
MITOX, PBS (pH 7.4)	610	661	0.87	685	58	0.7
MITOX, PBS (pH 4.5)	610	661	0.95	685	58	0.8
MITOX, MeOH	615	667	1.19	686	58	2.9##
MITOX, MeOH:$CHCl_3$ 1:1	618	671	1.20	690	56	2.9##
MITOX, EtOH	620	673	1.36	692	49	2
MITOX, propanol	623	675	1.34	694	46	2.1
MITOX, Triton X-100¶¶	610	661	1.18	685	54	2.1##
MITOX-DNA (1/17 bp)	628	680	1.34	700	50	0.65##
MITOX-RNA (1/14 bp)	626	678	1.34	688	61	
MITOX-RNA (1/29 bp)	627	679	1.34	690	56	
MITOX-DNA-topo II				700	50	0.65##
MITOX-topo II				685	58	1.0##
NQX, PBS (pH 7.4)	587	631	0.75	652§§	46§§	
NQX, dioxane	588	636	1.2	652	36	

*Concentrations of the components and experimental conditions are described in Materials and Methods.
#Intensities were corrected for the effect of inner filter. Excitation wavelength 514.5 nm.
§The ratio of absorbance at λ_{max2} to that at λ_{max1}.
¶Full width of spectrum at the half of maximum.
‖Relative intensity as compared with the intensity of equimolar aqueous solution of monomeric MITOX.
**Calculated using the data from (Kapuscinski and Darzynkiewicz, 1985).
##Corrected for the concentration of the monomeric MITOX in the solution studied.
§§Contribution of mitoxantrone signal was subtracted.
¶¶Concentration of Triton X-100 is equal to 0.24 mM.

the drug dissolved in different solvents. A moderate increase in hydrophobicity (methanol < methanol:chloroform < ethanol < propanol) was found to correlate with a progressing red-shift of the fluorescence emission and absorption maxima of the drug (Table 1). The red-shift of the emission maximum is accompanied by a decrease in the spectrum bandwidth (Table 1).

Because the shapes of the fluorescence excitation and absorption spectra of the drug are similar, and the latter has a R_A ratio of ~1.34 (Table 1), MITOX could be concluded to exist in a monomeric form in ethanol and propanol solutions. Similar reasoning shows that MITOX is less aggregated in methanol and methanol:chloroform solutions compared to the aqueous solution. Therefore, increasing environmental hydrophobicity induces dissociation of the drug's dimers. In addition, an elevation of fluorescence intensity by approximately twofold was detected for monomeric MITOX in ethanol and propanol solutions, as compared to the aqueous buffer solution at 514.5-nm excitation.

The ability of MITOX to penetrate the hydrophobic regions of vesicles and membranous structures was estimated by mixing MITOX with detergent micelles. The fluorescence emission spectrum of the drug is not changed in solutions containing Triton X-100 micelles, except for enhancement of intensity. Taking into account an increase in the R_A ratio to 1.18 (Table 1), dissociation of the dimers caused by interaction of MITOX with the detergent micelles can be assumed. Because this interaction does not induce a red-shift of the emission spectrum, there is no increase in environmental hydrophobicity. Therefore, the binding of MITOX occurs at the micelle surface without penetration of the drug molecule into the hydrophobic region of the micelle. Formation of hydrogen bonds between amino groups of MITOX and hydroxyl groups of the detergent molecules is the most probable mode of binding. As for the approximately twofold enhancement of fluorescence (Table 1), it seems that interactions of the amino groups with the micelle molecules eliminate the partial quenching of the fluorescence of chromophore moiety by the amino groups that occurs for the free molecules. It is known (Burstein, 1976) that external amino groups quench chromophore fluorescence in solution, whereas interactions of these groups (deprotonation, intermolecular hydrogen binding, etc.) eliminate quenching and enhance fluorescence.

The results suggest that MITOX weakly penetrates hydrophobic structures. Nevertheless, forced contacts with hydrophobic groups or domains may be expected at the cellular level. Some unprofitable (in terms of entropy) hydrophobic interactions seem to be possible if compensated for by electrostatic interactions and/or hydrogen binding of MITOX to polar or negatively charged groups of the surrounding molecules. This conclusion is confirmed by a red-shift of the fluorescence emission when MITOX was mixed with Triton X-100 at an enormous concentration of

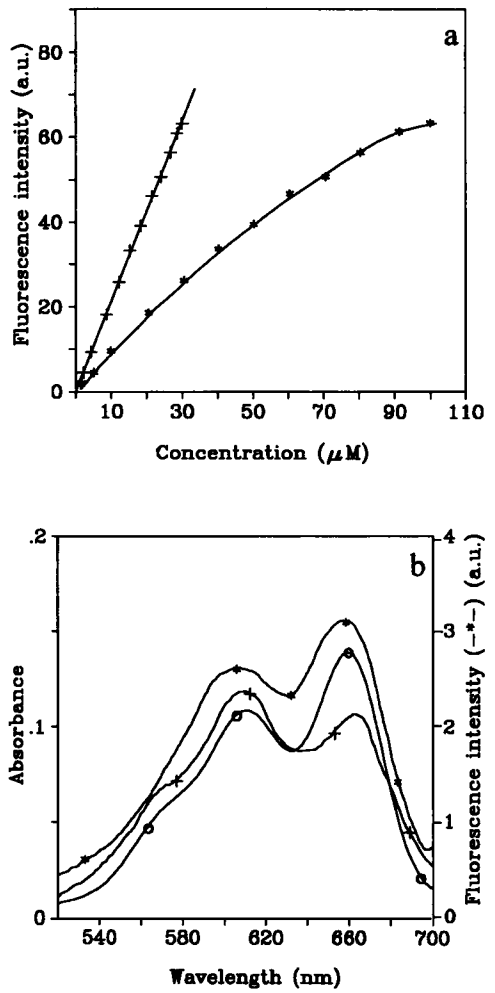

FIGURE 2 (*a*) Dependencies of the fluorescence intensity on the total concentration of MITOX (asterisks) and on the concentration of monomeric MITOX (+) in the PBS solution, pH 7.4. (*b*) Absorption (+) and fluorescence excitation (*) spectra of 10 μM MITOX solution in PBS (pH 7.4) as well as simulated (according to the data of Kapuscinski and Darzynkiewicz, 1985) absorption spectrum of monomeric MITOX (○) in aqueous solution. The dependence of intensity on the total concentration of MITOX was measured by microspectrofluorometry and corrected for the effect of the inner filter. The concentration of monomeric MITOX was calculated using the dimerization constant $K_d = 3 \times 10^4\ M^{-1}$ (Kapuscinski and Darzynkiewicz, 1985).

the detergent (50 mM, data not shown). In this case laminar structures rather than uniform micelles were formed in the aqueous solution. Multiple contacts of MITOX molecules with the hydrophobic regions of detergent laminar structures should be realized and may be responsible for the red-shift of the drug fluorescence.

Interactions with DNA and RNA

MITOX binds to double-stranded (ds) nucleic acids via intercalation (Kapuscinski and Darzynkiewicz, 1985; Reszka et al., 1989). Apart from intercalation, electrostatic interactions are known to occur between DNA phosphate groups and aminoalkylamino side chains of MITOX (Durr et al., 1983; Kapuscinski and Darzynkiewicz, 1986). Analysis of CD spectra (not shown), which is based on the CD spectra of different forms of DNA (Ivanov, 1973), reveals that an increase in a drug/bp ratio from 1/100 to 1/5 is accompanied by unwinding of the DNA helix. Finally, precipitation of the drug-DNA complex occurs at drug/bp ratios higher than 1/5.

The absorption spectrum of the drug-DNA complex is red-shifted and less intense as compared to the spectrum of free monomeric MITOX (Kapuscinski and Darzynkiewicz, 1985). Drug-DNA interaction causes a considerable red-shift of the fluorescence maximum, changes in the shape and bandwidth of the fluorescence spectrum (Table 1), as well as a decrease in fluorescence intensity (~35%). Fluorescence parameters of the drug-DNA complexes were found to be independent for a drug/bp ratio in the range from 1/100 to 1/5 (data not shown). It means that the contribution of a free drug to the spectrum of the drug-DNA complex is negligible at each drug/bp ratio used. This fact can be explained as follows:

1. A 20-fold increase in the drug/bp ratio leads to only 1.67-fold growth of the relative concentration of the free drug (from 8.4% to 14% of C_{tot}), according to the binding constant of $K = 2.52 \times 10^5\ M^{-1}$ published elsewhere (Kapuscinski and Darzynkiewicz, 1985).

2. Quenching of fluorescence of the free drug occurs because of nonradiative energy transfer from the molecule to the drug/DNA complex. The energy transfer is very effective, because the emission spectrum of the free drug (λ_{max} = 685 nm) extensively overlaps the excitation spectrum of the drug-DNA complex (λ_{max} = 680 nm).

MITOX was also found to bind with RNA. On interaction with RNA, the emission spectrum broadens and red-shifts (Table 1) as a function of a drug/bp ratio. The spectrum decomposition procedure indicates that the spectrum of the MITOX-RNA complex can be considered as a superposition of the spectra of free MITOX and MITOX-DNA complex. Analysis of CD spectra of the drug-RNA complexes (not shown), which is based on the CD spectra of different forms of RNA and DNA (Ivanov, 1973), reveals that 1) calf liver RNA has the structure of a ds helix, and 2) unwinding of RNA helix occurs as the drug/bp ratio increases.

These data allow a similar mode of drug interaction with both ds RNA and ds DNA to be suggested. The strong contribution of free MITOX to the spectrum of the drug-RNA complex can be explained by weaker binding of the drug to RNA versus DNA, stemming from the differences in the structure of double-stranded helixes of these biopolymers (Saenger, 1984).

Native RNA is recognized to form either a long ds helix or a single-stranded globular structure, according to its biological function. In the latter case, short double-stranded fragments are developed under folding of the RNA single chain into a globule (Saenger, 1984). Therefore, the intercalation binding mode, which is stabilized by electrostatic interactions involving anionic groups of RNA and amino

groups of the side chains of MITOX, can be expected for either type of RNA.

Modeling the drug interactions with DNA topoisomerase II

Formation of cleavable complexes between MITOX, topo II, and DNA does not induce any new spectral changes, as compared to the fluorescence emission spectrum of the MITOX-DNA complex (Table 1). The fluorescence spectrum of the drug is not perturbed by the addition of topo II to MITOX alone. It can be concluded that the chromophore moiety of MITOX is unable to interact with topo II alone, and intercalation of DNA should be considered as a first step toward the formation of the cleavable complex. Moreover, interaction of the chromophore with DNA (namely, its intercalation) is unaffected by binding of topo II to the drug-DNA complex. It should be mentioned that the data obtained agree with the generally accepted mechanism of the cleavable complex formation in the presence of topo II poisons (D'Agra and Liu, 1989). At the same time, the data of fluorescence spectroscopy do not preclude the interactions of the aminoalkylamino side chains of MITOX with topo II alone or within the ternary cleavable complex, because such interactions hardly affect the fluorescence of the chromophore moiety.

Spectral features of the naphtoquinoxaline metabolite of mitoxantrone

The absorption and fluorescence emission spectra of the NQX metabolite are blue-shifted compared to those of MITOX (Table 1). The fluorescence emission spectrum of the NQX metabolite narrows in dioxane versus the aqueous buffer, but no shift of the maximum occurs (Table 1). The absorption spectrum of the NQX metabolite is slightly red-shifted in dioxane. The R_A value (Table 1) points to the dissociation of NQX dimers in dioxane as compared to the state of the NQX metabolite in aqueous buffer. The NQX metabolite has both proton-accepting and proton-donating sites (Fig. 1), and its H-bonding state is different in dioxane, an acceptor solvent, as related to that in the aqueous buffer. Hence hydrogen bonding of NQX to the proton-accepting sites of dioxane molecules is responsible for the narrowing of the fluorescence spectrum.

Microspectrofluorometry of K562 cells treated with mitoxantrone

Intrinsic fluorescence of cells

The intensity of the cellular fluorescence was found to vary within different cellular compartments (Fig. 3). The nucleus does not fluoresce when excited at 514.5 nm, but intense fluorescence was observed from within cytoplasmic compartments of the cells. The strongest intrinsic cellular fluorescence was detected from cytoplasmic regions adjacent to the nucleus. The shape of the fluorescence spectra turned out to be the same in every fluorescent region of cytoplasm (Fig. 3 *c*). The spectra are broad. They have two overlapped maxima at 640 and 652 nm, as well as a shoulder at ~700 nm (Fig. 3 *c*, *curve 4*). The shape of the intrinsic fluorescence spectra was found to persist in the drug-treated cells.

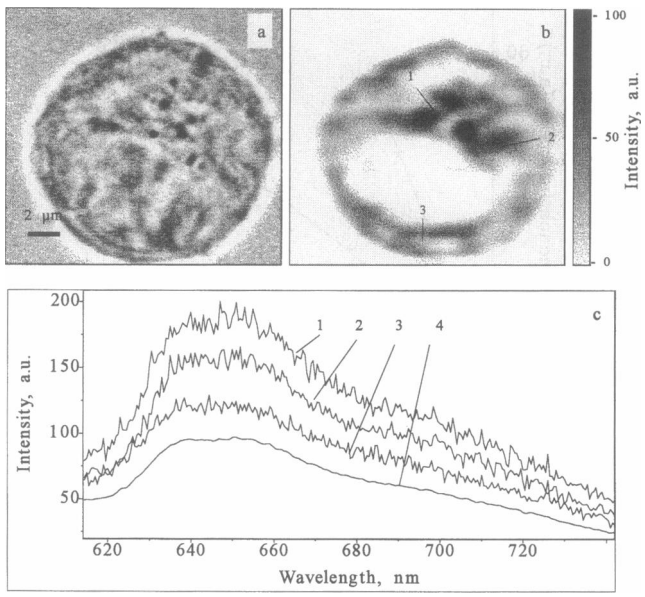

FIGURE 3 (*a*) Conventional light-microscope image of the cell. (*b*) Confocal spectral image of this cell created basing on the integral signal of intrinsic cellular fluorescence excited at the 514.5 nm wavelength. (*c*) Spectra of the intrinsic fluorescence of the cell (*curves 1–3*) recorded from within different cytoplasmic compartments. The regions from which the spectra were recorded (*curves 1–3*) are marked on the confocal spectral image of the cell. *Curve 4*, Integral spectrum of the intrinsic fluorescence of the cell constructed by averaging of the intrinsic fluorescence spectra from different cellular compartments.

Analysis of the spectra recorded from mitoxantrone-treated cells

The spectra recorded from different regions of MITOX-treated cells were found to differ in intensity, shape, width, and the position of the maximum (Fig. 4). Because these distinctions were obviously related to intracellular interactions of MITOX, their origin was identified by using the results of in vitro experiments. The spectra of MITOX disposed within nucleoli or perinucleolar regions of the nucleus were found to coincide with the spectrum of the MITOX-DNA complex with a small contribution of the monomeric drug (Fig. 4 *a*). The spectra from within some cytoplasmic compartments were well simulated by the spectrum of MITOX in propanol solution (Fig. 4 *b*). The spectra characteristic of the monomeric MITOX in aqueous environment were detected in other cytoplasmic compartments (Fig. 4 *d*). A narrow maximum was observed at 652 nm in the spectra recorded from within extranuclear compartments (Fig. 4, *c* and *d*). As discussed below, the unique parameters (position of maximum and width) of this band coincide with the spectrum of the NQX metabolite of MITOX in dioxane.

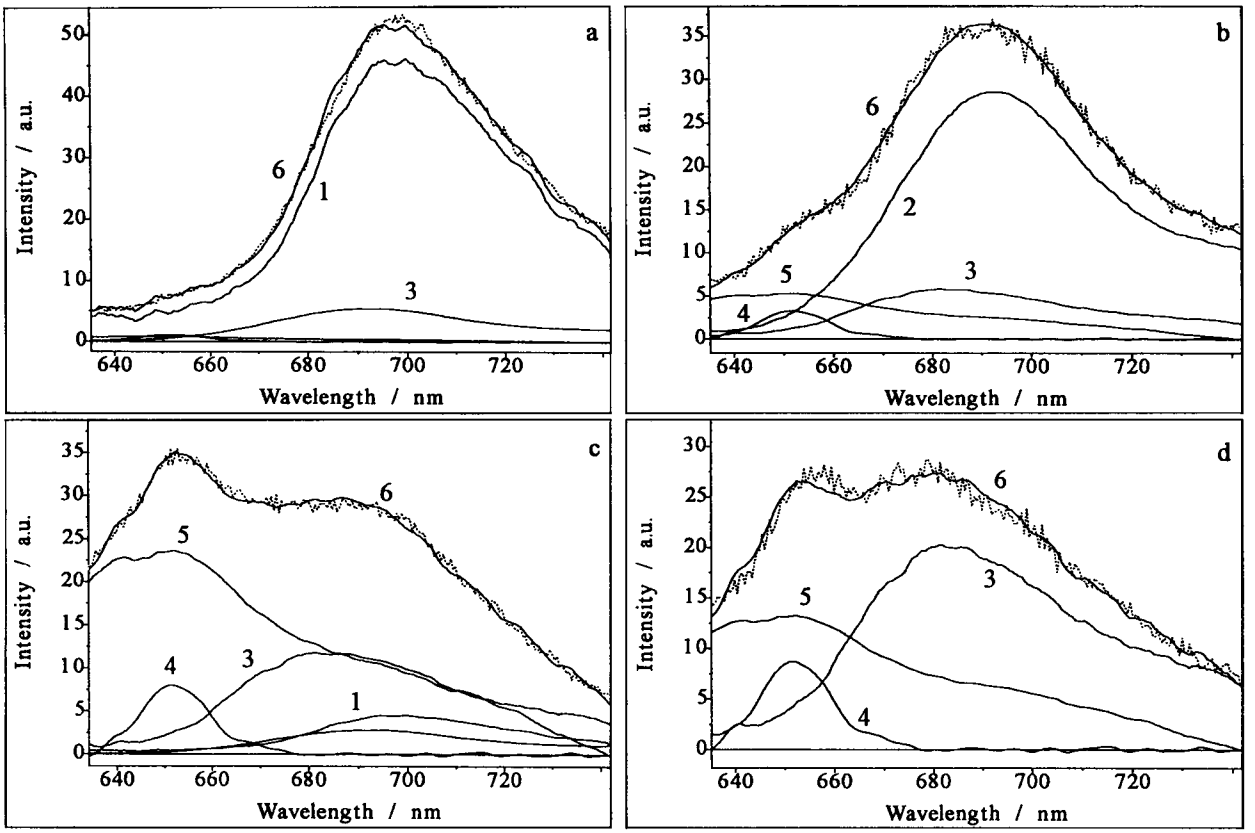

FIGURE 4 Several examples of the spectral analysis (decomposition procedure) of microfluorescence spectra (·····) recorded from within the nucleus (*A*) and different cytoplasmic compartments (*B–D*) of MITOX-treated cells. The decomposition of measured spectra into components was performed using the set of in vitro measured model spectra, which describe (*curve 1*) nucleic acid-related complexes of MITOX, (*curve 2*) MITOX in a hydrophobic environment, (*curve 3*) monomeric MITOX in polar environment, (*curve 4*) NQX metabolite bound to the ligands, as well as (*curve 5*) the intrinsic cellular fluorescence signal. The validity of the decomposition procedure can be estimated by comparing the spectra (*curve 6*) simulated on the basis of components 1–5 with the experimental spectra (·····). Spectra 1–5 show the relative contribution of each component to the overall spectrum.

The intrinsic cellular fluorescence contributes fairly well to the overall signal (Fig. 4, *c* and *d*), especially when a low concentration of the drug is used for treatment. Typically, the spectra appeared as a superposition of different signals (Fig. 4 *c*), which were assigned by means of the decomposition procedure.

The comprehensive analysis of the spectra recorded from the MITOX-treated cells permitted us to define a set of the reference spectra suitable for describing the state and interactions of MITOX in the K562 cells. This set includes 1) the spectrum of monomeric MITOX in an aqueous environment, 2) the spectrum of MITOX in propanol, 3) the spectrum of the MITOX-DNA complex, 4) the spectrum of the NQX metabolite in dioxane, and 5) the spectrum of the intrinsic cellular fluorescence.

Spectrum 2) may be considered to describe forced hydrophobic contacts and/or the nonpolar environment of MITOX bound to hydrophobic cellular structures. Spectrum 3) allows simulation of the complexes between MITOX and DNA, including ternary complexes between MITOX, DNA, and topo II in cells. Moreover, intercalation of MITOX in the ds fragments of RNA is readily modeled by this spectrum, as it follows from our in vitro experiments. Spectrum 4) is introduced to feature the distribution of the NQX metabolite within the cells.

Spectral images were recorded from more than 30 cells treated with both high (10 μM) and low (2 μM) concentrations of MITOX. Every spectral pattern of MITOX in the K-562 cells was examined and found to be well simulated, based on the set of reference spectra. The average error of the decomposition procedure was estimated to be 5–7%.

Spectral detection of NQX metabolite in K-562 cells

Microfluorescence spectra (λ_{exc} = 514.5 nm) recorded in the cytoplasmic region of the K562 cells treated with MITOX have a narrow maximum at 652 nm (Fig. 4, *c* and *d*. This spectral feature was obviously drug-related, because it was absent from the spectra recorded from control cells (Fig. 3 *c*), and its intensity correlated with a concentration-dependent increase in the intracellular MITOX signal. At the same time, this feature was not observed in modeling environmental effects and interactions of MITOX with possible molecular targets in vitro. It was proposed that it corresponds to one of MITOX metabolites. Among 11 metabolites of MITOX found in HepG2 hepatoma cells, the

only NQX metabolite has an absorption spectrum that blue-shifted by 30 nm compared to the MITOX spectrum (Mewes et al., 1993). Thereby, we predesignate the metabolite as a source of the peak at 652 nm. Absorption spectra of all other metabolites were reported to be red-shifted (Mewes et al., 1993). The NQX metabolite obtained in vitro as a result of MITOX oxidation catalyzed by horseradish peroxidase exhibits a fluorescence emission maximum at 652 nm (Table 1), thus coinciding with the maximum of the band under consideration.

To detect selectively the signal corresponding to the 652 nm feature, the microfluoresence spectra of drug-treated cells were recorded at the 488-nm excitation. A contribution of MITOX itself decreased, and a narrow 652-nm band was observed only in these spectra, yet it coincided (width, shape, and position of maximum) with the spectrum of NQX in dioxane. Taken together, these results permitted us to assign the 652-nm band in the microfluorescence spectra of the drug-treated cells to the NQX metabolite of MITOX.

The state of the NQX metabolite in the cellular environment is modeled by its spectrum in dioxane rather than in the aqueous solution. Therefore, the NQX metabolite is bound to the acceptor groups of cellular structures or molecules within the cytoplasmic region of the cells.

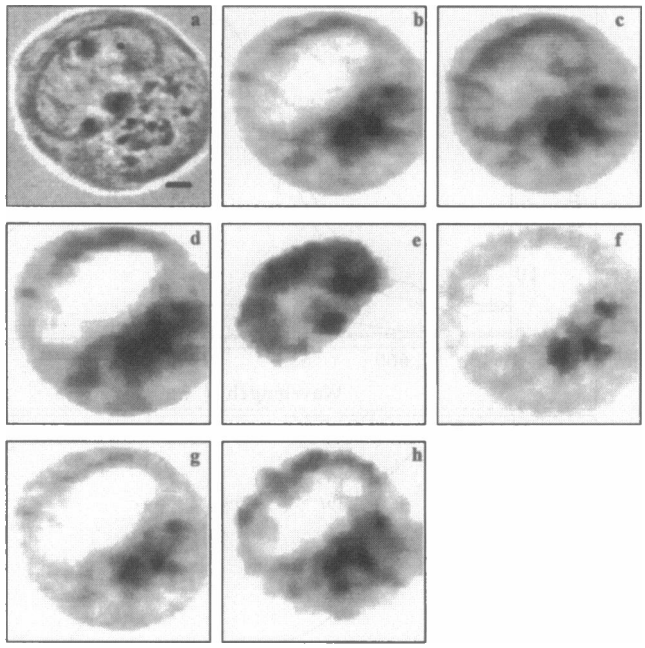

FIGURE 5 Confocal spectral images of the cell exposed to 10 μM MITOX concentration for 1 h. (*a*) Conventional light-microscope image of the cell. (*b*) Band-pass image (650 ± 5 nm). (*c*) Band-pass image (690 ± 5 nm). (*d–h*) Spectral images describing the distribution of monomeric MITOX in the aqueous intracellular environment (*d*), nucleic acid related complexes of MITOX (*e*), MITOX bound to the hydrophobic cellular structures (*f*), NQX metabolite bound to the ligands (*g*), and the intrinsic cellular fluorescence signal (*h*). The bar in *a* corresponds to 2 μm.

Confocal spectral images of mitoxantrone in K562 cells

The confocal spectral images were recorded from the equatorial optical sections of cells. The layer of 3-μm thickness contributed to the collected signal. The 514.5-nm excitation was used to record confocal spectral images, because the NQX metabolite, monomeric MITOX in an aqueous intracellular environment, MITOX bound to hydrophobic cellular structures, and complexes of MITOX with DNA may be simultaneously detected and mapped at this excitation (Fig. 5). Spectral images based on the fluorescence signal integrated over the selected spectral range (so-called band-pass images) were also created for comparative purposes. They are analogous to conventional LSCFM images, but in the former case, the width and position of spectral range used as a band-pass filter may be widely varied.

In accordance with the observations made previously by the LSCFM technique for SV40 transformed human fibroblasts (Smith et al., 1992) the integral fluorescence signal of MITOX was detected from within the cytoplasm, nuclear membrane, and nucleoli of K562 cells (Fig. 5, *b* and *c*). Nevertheless, both enhancement of fluorescence in nonpolar environment and partial fluorescence quenching of MITOX bound to DNA distort the drug disposition that appears in confocal spectral band-pass images (Fig. 5, *b* and *c*) and LSCFM images (Smith et al., 1992). Moreover, the intrinsic cellular fluorescence introduces a perceptible contribution to the integral signal, especially when a low drug concentration is used for cell treatment. Both a complicated shape of the spectrum and overlapping with the spectra of the drug make it impossible to account for the intrinsic cellular fluorescence contribution to the overall signal in band-pass images.

By decomposing the intracellular spectra into reference spectra of MITOX in different states and correcting for enhancement and quenching of corresponding signals, the real pattern of the drug disposition is revealed, and moreover, the features of the drug interactions are clearly observed (Fig. 5, *d–g*). Because the spectra heavily overlap, these interactions cannot be identified in band-pass images, regardless of the spectral region chosen to integrate signal.

Monomeric MITOX in an aqueous microenvironment, MITOX bound to hydrophobic cellular structures, and the NQX metabolite are distributed throughout the cytoplasm, whereas the presence of the MITOX-nucleic acid complexes in cytoplasm is quite negligible (Fig. 5, *d*, *f*, *g*). The overall signal of the drug within the nucleus is undoubtedly related to the drug-DNA complexes, with contributions from the MITOX-DNA-topo II and MITOX-RNA complexes (Fig. 5 *e*). Perinucleolar staining and increased accumulation of MITOX in nucleolar-like bodies are detected. The patterns of subcellular distribution of monomeric MITOX located in an aqueous environment and the NQX metabolite have similar features: besides the drug being uniformly distributed in the cytoplasm, compact regions of drug accumulation are observed near the nucleus. The regions of concentrated MITOX and the NQX metabolite coincide with the sites of intense intrinsic cellular fluores-

cence. General staining of hydrophobic cellular structures and capture of the drug in small hydrophobic inclusions are apparent in the cytoplasmic region of the cells for MITOX (referred to as bound to hydrophobic cellular structures).

The distribution of the drug along the equatorial optical section was compared to 3D distribution of the drug within the cell. The 3D analysis was performed by measuring the spectral images at different optical sections of the cell (at different positions of the focal plane). Three series of confocal spectral images of the cell obtained at the equatorial optical cross section, and at 3 μm and 6 μm above it, are presented in Fig. 6. The 3D analysis reveals similar features of the drug distribution and interactions as described above for the equatorial cross sections.

DISCUSSION

Recently Smith et al. (1992) presented the LCSFM images of MITOX distribution within SV40 transformed human fibroblasts. This study was based on the analysis of integral fluorescence signal of the drug. Here we present the first attempt to characterize the features of subcellular distribution of both MITOX and its complexes with cellular structures within intact, living K562 cells. For this purpose, microfluorescence confocal spectral imaging analysis combined with detailed in vitro modeling experiments was performed.

Adequate in vitro modeling plays a key role in the interpretation of the data, because the drug-associated intracellular fluorescence may be affected by a number of multiple factors, including ionic composition, pH, and polarity of the environment, as well as specific and nonspecific molecular interactions and metabolization of the drug within cellular organelles. These factors often lead to prominent changes in drug fluorescence, ranging from simple quenching or enhancement to remarkable shifts and changes in emission spectrum. Therefore, the question of whether the fluorescence of the drug reflects its intracellular accumulation, subcellular distribution, and interactions is important in applications of flow cytometry, LCSFM, and CSI techniques to analysis of the drug within living cells. Because so far this question has not been elucidated for MITOX, we performed a series of in vitro experiments to examine the influence of different environmental factors and drug interactions with potential intracellular targets on the fluorescence of MITOX.

The following effects and characteristics were observed:

1. dramatic quenching of drug fluorescence when the drug was in the form of self-aggregates;
2. a characteristic spectral shift and enhancement of the fluorescence of the drug when it was in a hydrophobic environment;
3. a characteristic spectral shift and moderate quenching of the fluorescence of the drug if it was complexed to nucleic acids;
4. characteristic spectral features of the NQX metabolite of MITOX.

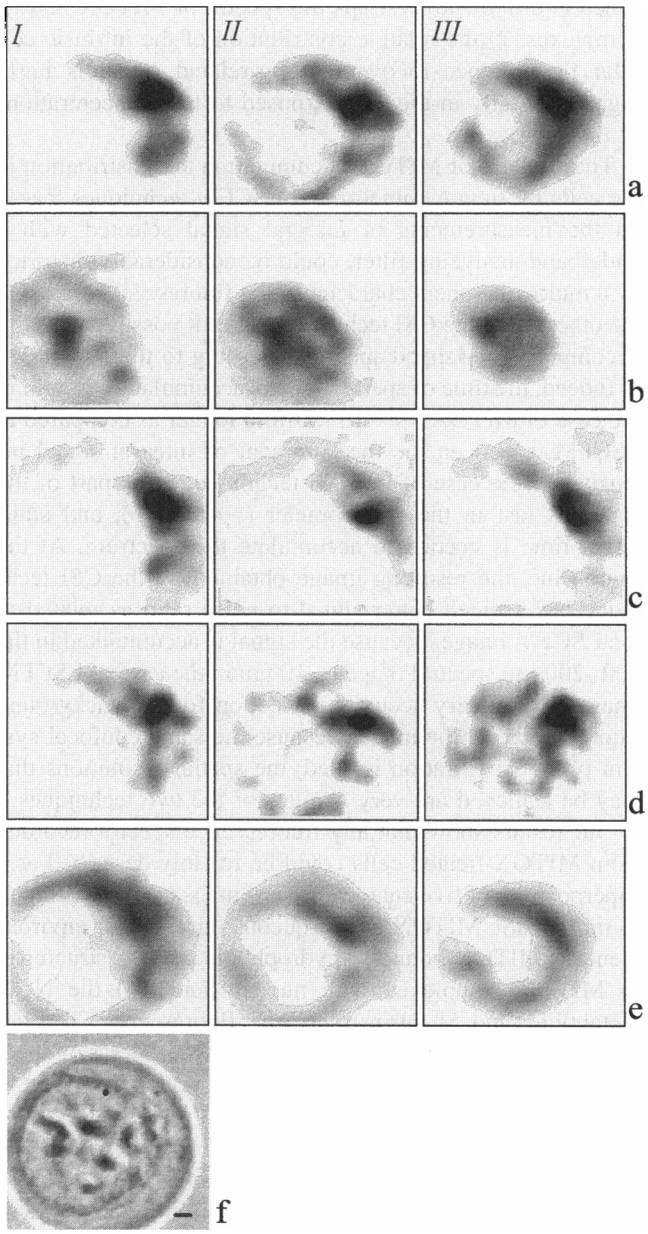

FIGURE 6 Confocal spectral images of the cell measured (*I*) at the equatorial optical cross section, and 3 μm (*II*) and 6 μm (*III*) above the equatorial cross section. The cell was exposed to 10 μM MITOX concentration for 1 h. (*a–e*) Spectral images describing the distribution of intrinsic cellular fluorescence signal (*a*), nucleic acid-related complexes of MITOX (*b*), monomeric MITOX in the aqueous intracellular environment (*c*), NQX metabolite bound to the ligands (*d*), and MITOX bound to the hydrophobic cellular structures (*e*). (*f*) Conventional light-microscope image of the cell. The bar in *f* corresponds to 2 μm.

All of these factors affecting the signal of MITOX should be taken into account to reveal the real pattern of the drug distribution and interactions within the cells.

Another important factor influencing measurements is derived from intrinsic fluorescence properties of cells. The results obtained for control and MITOX-treated K562 cells show that 1) the spectrum of the intrinsic cellular fluores-

cence is broad and overlaps the spectra of MITOX and its complexes, 2) the relative contribution of the intrinsic cellular fluorescence to overall drug-related signal is fairly high, especially in the cells exposed to low concentrations of the drug.

The analysis of MITOX accumulation and distribution in the cells by flow cytometry and LSCFM techniques, based on the measurements of integral signal selected with a wide-band analyzing filter, could be considerably distorted by a multicomponent character of the fluorescent signal. On the other hand, the CSI technique makes it possible to easily decompose overlapped spectra according to their origin.

Indeed, the time of spectral image accumulation (4 min in the case of MITOX) is ~10–20-fold longer as compared to LSCFM, based on the measurement of integral signal intensity. In the case of the CSI technique, some part of the signal is lost in the spectrometer (~40–50%), and additional time is needed to accumulate the spectrum. At the same time, the resulting image obtained by the CSI technique has a much better signal-to-noise ratio as related to the LSCFM image, because the signal is accumulated in the 100–200-nm spectral range (~10 nm in the case of LSCFM image), and a very accurate correction for the background fluorescence can be made. Because the same confocal system of signal filtration is used, the spatial resolutions that may be achieved are very similar for the two techniques.

Our results show that any fluorescence spectra recorded from MITOX-treated cells could be reliably described as a superposition of five characteristic signals, corresponding to 1) monomeric MITOX in an aqueous intracellular environment, 2) MITOX bound to hydrophobic cellular structures, 3) MITOX complexed with nucleic acids, 4) the NQX metabolite, and 5) intrinsic cellular fluorescence. The decomposition procedure being applied to the 2D set of spectra allows the subcellular distribution of each component to be mapped.

In addition, the 3D analysis was performed to clarify and prove the features of the drug interactions. Generally, by measuring confocal spectral images at different positions of the focal plane along the z axis, a 3D model of intracellular localization may be created for each component. At the same time, it is necessary to ensure that the living cell and distribution of the drug are not disrupted under irradiation. Therefore, reconstruction of the complete 3D model is restricted to the number of consequent measurements that does not disturb the living cell and intracellular distribution of the drug. In our experimental conditions, the 3D analysis was restricted to five to seven measurements at the different optical cross sections. For longer periods of irradiation, cells were found to lyse. Although this number of measurements was not enough to reconstruct a detailed 3D image, the main features of localization and interactions of MITOX were revealed. The 3D analysis confirms the data obtained when the equatorial optical cross sections of cells were measured. Therefore, all statistically important features of distribution and interactions of the drug may be found by analyzing comparatively different cells and averaging the data obtained at the equatorial optical cross sections of a number of the cells.

Three different states of MITOX can be traced in living cells to micron resolution. Two of them, MITOX-nucleic acid complexes and MITOX bound to hydrophobic cellular structures, are suggested to be directly involved with the antitumor action of the drug (Smith et al., 1990; Kapuscinski and Darzynkiewicz, 1986; Roberts et al., 1989; Ho et al., 1991). Furthermore, the NQX metabolite of MITOX was detected in the K562 cells and its subcellular distribution was established. The CSI technique has the advantage of allowing this metabolite to be detected in the cells simultaneously with its parent compound, MITOX, and with complexes formed by MITOX within the cellular structures and molecules. Therefore, the dynamics and molecular mechanism of MITOX metabolization can be studied. Moreover, particular functions of metabolites (at least the NQX one), MITOX bound to hydrophobic cellular structures and drug-DNA complexes in the antitumor action of MITOX, can be clarified with the help of CSI analysis. Quantitative analysis of subcellular accumulation and distribution of MITOX and drug-target complexes should precede the study of the mechanisms, and it is the subject of our following paper.

We are grateful to A. Kokota for excellent software assistance and to H. Morjani for assistance with cell manipulations. We also thank all of the people who helped us at the DILOR S.A. (Lille, France). We are particularly grateful to M. Manfait for providing stimulating discussions during the course of this study and manuscript preparation. We thank E. Kryukov for critical reading of the manuscript and correction of the English.

This research was supported by grants from the Russian Foundation for Basic Research (96-04-48421) and 1379 from the Association pour la Recherche Contre le Cancer (France). AF was supported by a FEBS short-term fellowship.

REFERENCES

Arlin, Z., D. C. Case, J. Moore, P. Wiernik, E. Feldman, S. Saletan, P. Desai, L. Sia, and K. Cartwright. 1990. Lederle Cooperative Group: randomized multicenter trial of cytosine arabinoside with mitoxantrone or daunorubicin in previously untreated adult patients with acute nonlymphocytic leukemia (ANLL). *Leukemia.* 4:177–184.

Burstein, E. A. 1976. Luminescence of protein chromophores (model studies). *In* Biophysics, Vol. 6. Yu. A. Vladimirov, editor. VINITI, Moscow.

D'Agra, P., and L. F. Liu. 1989. Topoisomerase-targeting antitumor drugs. *Biochim. Biophys. Acta.* 989:163–177.

Durr, F. E., R. W. Wallace, and R. V. Ciatarella. 1983. Molecular and biochemical pharmacology of mitoxantrone. *Cancer Treat. Rev.* 10(Suppl):3–11.

Ehninger, G., U. Schuler, B. Proksch, K.-P. Zeller, and J. Blanz. 1990. Pharmacokinetics and metabolism of mitoxantrone. A review. *Clin. Pharmacokinet.* 18:365–380.

Faulds, D., J. A. Balfour, P. Chrisp, and H. D. Langtry. 1991. Mitoxantrone. A review of its pharmacodynamic and pharmacokinetic properties, and therapeutic potential in the chemotherapy of cancer. *Drugs.* 41:400–449.

Feofanov, A., S. Sharonov, P. Valisa, E. Da Silva, I. Nabiev, and M. Manfait. 1995. A new confocal stigmatic spectrometer for micro-Raman and microfluorescence spectral imaging analysis: design and applications. *Rev. Sci. Instrum.* 66:3146–3158.

Fujimoto, S., and M. Ogawa. 1982. Antitumor activity of mitoxantrone against murine experimental tumors: comparative analysis against various antitumor antibiotics. *Cancer Chemother. Pharmacol.* 8:157–162.

Gigli, M., S. M. Doglia, J. M. Millot, L. Valentini, and M. Manfait. 1988. Quantitative study of doxorubicin in living cell nuclei by microspectrofluorometry. *Biochim. Biophys. Acta.* 950:13–20.

Ho, C. K., S. L. Law, H. Chiang, M. L. Hsu, C. C. Wang, and S. Y. Wang. 1991. Inhibition of microtubule assembly is a possible mechanism of action of mitoxantrone. *Biochem. Biophys. Res. Commun.* 180:118–123.

Ivanov, V. I. 1973. Circular dichroism and structure of complementary nucleic acids. *In* Molecular Biology. M. V. Volkenstein, editor. VINITI/USSR, Moscow. V.1, 105–140

Johnson, R. K., R. K. Y. Zee-Cheng, W. W. Lee, E. M. Acton, D. W. Henry, and C. C. Cheng. 1979. Experimental antitumor activity of aminoanthraquinones. *Cancer Treat. Rep.* 63:425–439.

Kapuscinski, J., and Z. Darzynkiewicz. 1985. Interactions of antitumor agents ametatrone and mitoxantrone (Novatrone) with double-stranded DNA. *Clin. Pharmacol.* 34:4203–4213.

Kapuscinski, J., and Z. Darzynkiewicz. 1986. Relationship between the pharmacological activity of the antitumor drugs ametantrone and mitoxantrone and their ability to condense nucleic acids. *Proc. Natl. Acad. Sci. USA.* 83:6302–6306.

Kapuscinski, J., Z. Darzynkiewicz, F. Traganos, and M. R. Melamed. 1981. Interaction of a new antitumor agent, 1–4-dihydroxy-5,8-bis-[[2-(2-hydroxyethyl)-amino]ethyl]amino]-9,10-anthracenedione, with nucleic acids. *Biochem. Pharmacol.* 30:231–240.

Liyanage, M., A. Coleman, S. du Manoir, T. Veldman, S. McCormack, R. B. Dickson, C. Barlow, A. Wynshaw-Boris, S. Janz, J. Wienberg, M. A. Ferguson-Smith, E. Schrock, and T. Ried. 1996. Multicolour spectral karyotyping of mouse chromosomes. *Nature Genet.* 14: 312–315.

Malik, Z., M. Dishi, and Y. Garini. 1996. Fourier transform multipixel spectroscopy and spectral imaging of photoporphyrin in single melanoma cells. *Photochem. Photobiol.* 63:608–614.

McLean Grogan, W., and J. M. Collins. 1990. Guide to Flow Cytometry Methods. Marcel Dekker, New York.

Mewes, K., J. Blanz, G. Ehninger, R. Gebhard, and K.-P. Zeller. 1993. Cytochrome P-450-induced cytotoxicity of mitoxantrone by formation of electrophilic intermediates. *Cancer Res.* 53:5135–5142.

Nabiev, I., I. Chourpa, J.-F. Riou, C. H. Nguyen, F. Lavelle, and M. Manfait. 1994. Molecular interactions of DNA-topoisomerase I and II inhibitor with DNA and topoisomerases and in ternary complexes: binding modes and biological effects for intoplicine derivatives. *Biochemistry.* 33:9013–9023.

Pawley, J. B., editor. 1990. Handbook of Biological Confocal Microscopy. Plenum Publishing, New York.

Reszka, K., J. A. Hartley, P. Kolodziejczyk, and J. W. Lown. 1989. Interaction of the peroxidase-derived metabolite of mitoxantrone with nucleic acids. Evidence for covalent binding of ^{14}C-labeled drug. *Biochem. Pharmacol.* 38:4253–4260.

Reszka, K., P. Kolodziejczyk, and J. W. Lown. 1986. Horseradish peroxidase-catalyzed oxidation of mitoxantrone: spectrophotometric and electron paramagnetic resonance studies. *J. Free Radicals Biol. Med.* 2: 25–32.

Roberts, R. A., A. E. Cress, and W. S. Dalton. 1989. Persistent intracellular binding of mitoxantrone in a human colon carcinoma cell line. *Biochem. Pharmacol.* 38:4283–4290.

Saenger, W. 1984. Principles of Nucleic Acid Structure. Springer Verlag, New York.

Sharonov, S., I. Chourpa, H. Morjani, I. Nabiev, M. Manfait, and A. Feofanov. 1994a. Confocal spectral imaging analysis in studies of the spatial distribution of antitumor drugs within living cancer cells. *Anal. Chim. Acta.* 290:40–47.

Sharonov, S., I. Nabiev, I. Chourpa, A. Feofanov, P. Valisa, and M. Manfait. 1994b. Confocal three-dimensional scanning laser Raman-SERS-fluorescence microprobe. Spectral imaging and high-resolution applications. *J. Raman Spectrosc.* 25:699–707.

Smith, P. J., S. A. Morgan, M. E. Fox, and J. V. Watson. 1990. Mitoxantrone-DNA binding and the induction of topoisomerase II associated DNA damage in multi-drug resistant small cell lung cancer cells. *Biochem. Pharmacol.* 40:2069–2078.

Smith, P. J., H. R. Sykes, M. E. Fox, and I. J. Furlong. 1992. Subcellular distribution of the anticancer drug mitoxantrone in human and drug-resistance murine cells analysed by flow cytometry and confocal microscopy and its relationship to the induction of DNA damage. *Cancer Res.* 52:4000–4008.